

Single-cell analysis of olfactory neurogenesis and differentiation in adult humans

Michael A. Durante^{1,2,3,4,10}, Stefan Kurtenbach^{1,2,3,10}, Zoukaa B. Sargi^{4,5}, J. William Harbour^{2,3,4}, Rhea Choi^{1,2,6}, Sarah Kurtenbach^{2,5}, Garrett M. Goss^{2,5}, Hiroaki Matsunami^{7,8} and Bradley J. Goldstein^{1,2,5,6,9*}

The presence of active neurogenic niches in adult humans is controversial. We focused attention to the human olfactory neuroepithelium, an extracranial site supplying input to the olfactory bulbs of the brain. Using single-cell RNA sequencing analyzing 28,726 cells, we identified neural stem cell and neural progenitor cell pools and neurons. Additionally, we detailed the expression of 140 olfactory receptors. These data from the olfactory neuroepithelium niche provide evidence that neuron production may continue for decades in humans.

Mitotic tracing, fate mapping, and single-cell RNA sequencing (scRNA-seq) analyses have shown that rodent olfactory neuroepithelium supports ongoing neurogenesis through adulthood, that is, up to two years of age^{1–6}, but there has been little direct evidence to evaluate how well human olfactory neurogenesis may persist for the longer life span of many decades. Extrapolating from rodent studies, descriptive immunohistochemistry (IHC) using human olfactory neuroepithelium suggested that progenitors may be present, but also identified species-related differences^{7,8}. In addition, light microscopy examination of adult nonhuman primate olfactory neuroepithelium described basal cell pools, although ages were not specified⁹. To investigate the presence of true neurogenic progenitors and nascent neurons, we obtained fresh tissue samples from adult patients undergoing endoscopic nasal surgery involving resection of the anterior skull base or wide dissection for neurosurgical access ($n=7$ individuals). These cases provided access to normal olfactory cleft or turbinate tissue, which was uninvolved with any pathology but required removal (Supplementary Table 1). Samples were processed for scRNA-seq (four cases) and/or IHC.

After filtering, analysis of 28,726 single cells was performed (5,538–11,184 cells per case; Fig. 1, Extended Data Fig. 1 and Supplementary Table 2). Data were projected onto two dimensions via uniform manifold approximation and projection (UMAP) to analyze cellular heterogeneity^{10,11}. Cell type assignments for each cluster were generated using Gene Ontology and pathway analysis, using multiple known murine marker genes for horizontal basal cells (HBCs), globose basal cells (GBCs), immature and mature olfactory neurons, as well as Bowman's glands, olfactory neuroepithelium sustentacular cells⁵, endothelial/perivascular cells¹² or immune cells (Fig. 1b–d and Extended Data Fig. 1). While our samples comprised olfactory and respiratory mucosa, olfactory neuroepithelial cells clustered

distinctly from other cell types (Fig. 1a–c) and aggregated together in batch-corrected samples pooled from separate individuals (Fig. 1b,c). We hypothesized that, if ongoing neurogenesis is prominent in adult human olfactory neuroepithelium, a small subset of cells should express GBC proneural genes, as in rodents, and that immature neurons should be identifiable. Our results indicated that cell populations present in olfactory mucosa from adult individuals (age 41–52 years) contained several stages of neurogenic pools and immature neurons (Figs. 1d,e and 2 and Extended Data Figs. 2 and 3).

In the scRNA-seq data, immature neurons represented a surprisingly large proportion (55%) of all human olfactory neurons. In contrast, in adult nonlesioned rodent olfactory neuroepithelium, markers for immature neurons, such as TUJ1 or GAP43, label only about 5–15% of all olfactory neurons, based on widely published staining patterns.² Published high-quality murine scRNA-seq datasets analyzed cells from postnatal mice, thus limiting the ability for direct comparison⁵. In this study, we found that in human olfactory neuroepithelium, the G protein subunit guanine nucleotide-binding protein G(I)/G(S)/G(O) subunit gamma-8 (GNG8) is highly enriched in immature neurons, whereas GNG13 marks mature neurons, as described in the mouse⁵ (Fig. 1e,f). A subset analysis of olfactory neural lineage cell clusters, reprojected via UMAP, demonstrated the largely distinct expression patterns of GNG8 and GNG13 (Fig. 1e). In agreement, using IHC, GNG13 protein expression localizes to the mature olfactory neuron regions in both human and mouse olfactory neuroepithelia (Fig. 1f); a panel of IHC cell-type-specific markers identified abundant immature cells in the human olfactory neuroepithelium, indicating that a selective loss of mature cells during sample processing probably does not account for the scRNA-seq findings (Fig. 2). In addition, populations of resident or activated leukocytes were prominent in samples from all patients (Extended Data Fig. 4), suggesting the potential for immune responses to influence tissue homeostasis in the olfactory neuroepithelium, as shown in murine models of cytokine overexpression¹³.

Focusing attention on the olfactory populations, neurogenic GBCs, defined by the expression of basic helix-loop-helix transcription factors such as transcription cofactor HES-6 (HES6), neurogenin-1 (NEUROG1) or neurogenic differentiation factor 1 (NEUROD1), were a distinct cluster in the UMAP plots (see Figs. 1b,d,e and 2f), representing approximately 2% of all olfactory

¹Medical Scientist Training Program, University of Miami Miller School of Medicine, Miami, FL, USA. ²Interdisciplinary Stem Cell Institute, University of Miami Miller School of Medicine, Miami, FL, USA. ³Bascom Palmer Eye Institute, University of Miami Miller School of Medicine, Miami, FL, USA.

⁴Sylvester Comprehensive Cancer Center, University of Miami Miller School of Medicine, Miami, FL, USA. ⁵Department of Otolaryngology, University of Miami Miller School of Medicine, Miami, FL, USA. ⁶Graduate Program in Neuroscience, University of Miami Miller School of Medicine, Miami, FL, USA.

⁷Department of Molecular Genetics and Microbiology, Duke Institute for Brain Sciences, Duke University Medical Center, Durham, NC, USA. ⁸Department of Neurobiology, Duke Institute for Brain Sciences, Duke University Medical Center, Durham, NC, USA. ⁹Present address: Department of Head and Neck Surgery & Communication Sciences, Duke University Medical Center, Durham, NC, USA. ¹⁰These authors contributed equally: Michael A. Durante, Stefan Kurtenbach. *e-mail: bradley.goldstein@duke.edu

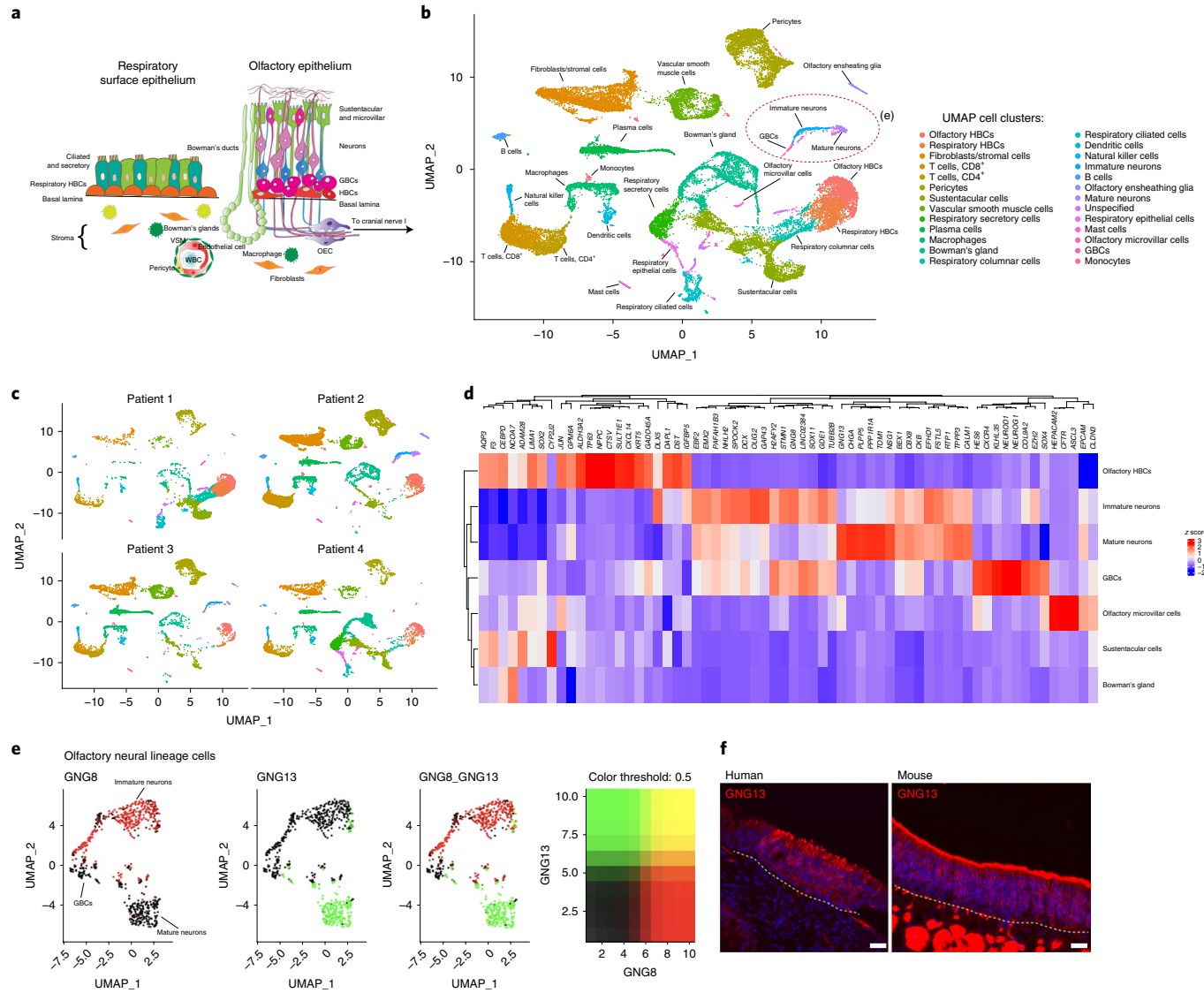


Fig. 1 | Aggregate analysis of 28,726 single cells from human olfactory cleft mucosa. **a,** Schematic diagram of respiratory versus olfactory epithelia. OEC, olfactory ensheathing cell; VSM, vascular smooth muscle (VSM); WBC, white blood cell. **b,** UMAP dimensionality reduction plot of 28,726 combined olfactory and respiratory mucosal cells; $n = 4$ patients. The cell cluster phenotype is noted on the color key legend and labels. **c,** Plots of individual patient samples; $n = 4$ patients. Patient 1: 5,683 cells; patient 2: 11,184 cells; patient 3: 5,538 cells; patient 4: 6,321 cells (see also Extended Data Fig. 1c). **d,** Heatmap depicting selected gene expression among olfactory cell clusters. **e,** UMAP depicting GNG8 and GNG13 expression in 694 GBCs and in immature and mature olfactory neurons; $n = 4$ patients. **f,** GNG13 immunostaining (red) in adult human and mouse olfactory neuroepithelia; the dashed line marks the basal lamina; nuclei are stained with DAPI (blue). Immunostaining was conducted in triplicate with similar results. Scale bar, 25 μ m.

neuroepithelium cells (see also Extended Data Fig. 5 and Supplementary Table 2). Differences in gene expression among the GBCs, and immature and mature neuron clusters are apparent in a DotPlot visualization (Fig. 2a), which also depicts the transition in marker expression from GBC to immature neuron to mature neuron, when focusing on transcription factors and olfactory transduction components. Additional data tables provide a resource of human olfactory neuroepithelium population gene expression lists (Supplementary Tables 3–6). Selected pathway analyses from differential expression data suggest chemosensory or progenitor cell phenotypes (Extended Data Fig. 6). To further verify the scRNA-seq findings, we compared human and mouse IHC using available validated antibodies for cell-type-specific markers (Fig. 2). IHC supported the conclusion that immature neurons, labeled by the antibody TUJ1 against the *TUBB* gene indicated on the DotPlot, are more numerous in our human olfactory neuroepithelium samples compared to adult mice (Fig. 2b).

Also, human samples often contained *KRT5*⁺/*SOX2*⁺ HBCs with a rounded or layered ‘reactive’ morphology, rather than the flat monolayer typical of quiescent mouse olfactory neuroepithelium (Fig. 2b,c). Reactive morphology HBCs are well described in the rodent olfactory neuroepithelium during injury-induced epithelial reconstitution^{3,14}. The proliferative GBC layer was visualized with anti-Ki67 and appears similar in human and mouse samples (Fig. 2d and Extended Data Fig. 2). Antibody to LIM homeobox protein 2 (*LHX2*), a transcription factor critically important in the regulation of olfactory receptor gene expression in differentiating olfactory neurons^{15,16}, brightly labels the nuclei of immature neurons and weakly labels the mature neurons, consistent with DotPlot expression patterns (Fig. 2e and Extended Data Fig. 3).

We focused further attention on olfactory receptor expression and detected the expression of 545 olfactory receptors across all neurons from 140 different olfactory receptor genes (Fig. 3 and Supplementary

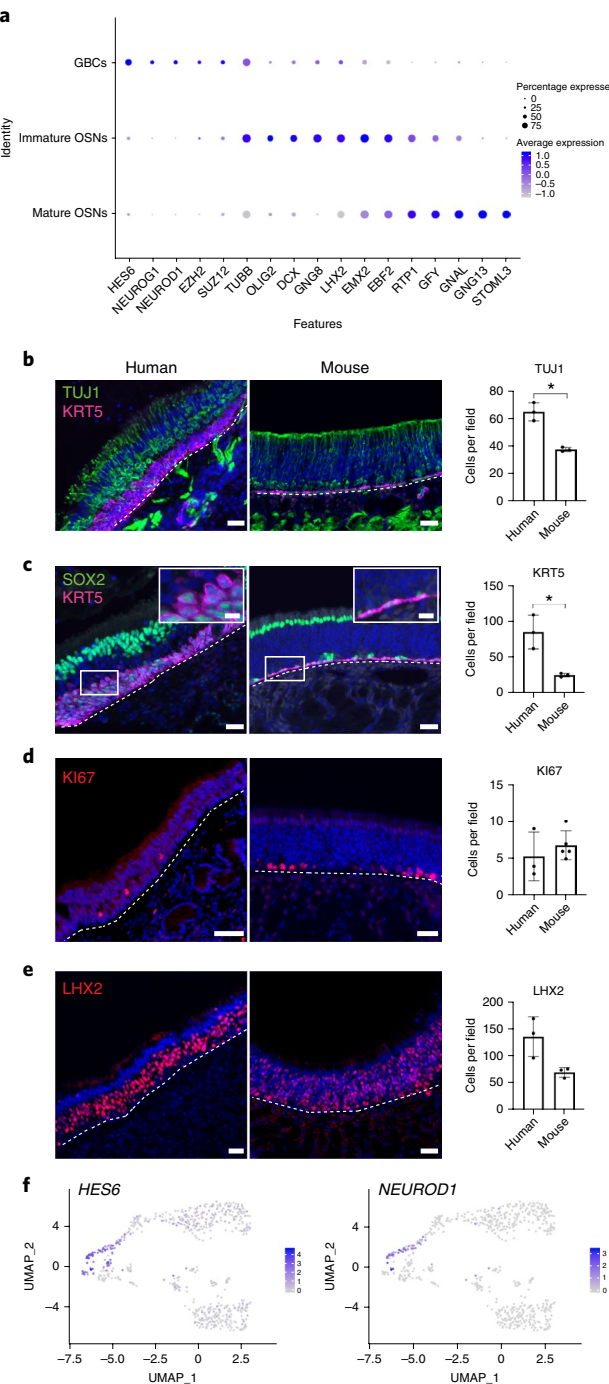


Fig. 2 | Gene expression analysis of human olfactory neuroepithelium. **a**, DotPlot visualization of neuron lineage cell populations from adult human olfactory neuroepithelium; $n = 4$ patients. **b**, Cell-type-specific marker validation in human versus mouse olfactory mucosal sections. TUJ1 labels the somata of immature OSNs, which are more abundant in our adult human samples ($n = 3$, two-sided Welch's t -test, $P = 0.015$). **c**, SOX2 marks the basal and sustentacular cells; KRT5 labels HBCs, which, in many areas of the human samples, have a reactive rather than flat morphology (inset, enlarged) and are abundant ($n = 3$, two-sided Welch's t -test, $P = 0.04$). **d**, KI67 marks proliferative GBCs. **e**, LHX2 was highly expressed in immature OSNs (DotPlot in **a**); IHC confirmed widespread expression in human cell populations and variable expression in mice. Nuclei are stained with DAPI (blue); the dashed line marks the basal lamina. * $P < 0.05$; the measure of center and error bars are the mean \pm s.d. Scale bar, 50 μ m; in inset (**c**), 10 μ m. **f**, Focused UMAP plots visualizing gene expression of HES6 and NEUROD1 in GBCs; $n = 4$ patients.

Tables 7–10). Excluding from the analysis transcripts with low relative expression (Extended Data Fig. 7a), our data included one mature neuron expressing the vomeronasal type-1 receptor 1 (VN1R1), whose ligand Hedione has been shown to elicit sex-specific human brain activity¹⁷ (Fig. 3a). Olfactory neuron identity was distinguished by coexpression of known olfactory transduction genes (see Fig. 2a); in the UMAP cell cluster labeled as ‘mature neurons’, 96% of cells express RTP1, 94% express GFY, 99% express GNAL and 96% express GNG13 (Fig. 2a and Supplementary Tables 3 and 5). In a subanalysis of the neuron cluster cells ($n = 668$) expressing GNG8⁺ (that is, immature) and/or GNG13⁺ (mature), 50% of GNG8⁺ cells expressed at least one olfactory receptor (Fig. 3b). In contrast, $>85\%$ of GNG13⁺/GNG8⁺ cells or GNG13⁺ cells expressed olfactory receptors. Significantly more immature olfactory sensory neurons (OSNs; 40%) did not express any olfactory receptors compared to mature OSNs (9.6%; Fig. 3b, $P < 0.05$). However, consistent with previous findings reporting that immature neurons are more likely to transiently express multiple olfactory receptors, since singular olfactory receptor choice is not yet stabilized¹⁸, we found that coexpression of >3 olfactory receptors was more often identifiable in immature OSNs compared to mature OSNs ($P = 0.01$). The ‘one-neuron/one-receptor’ rule^{19,20} appeared to generally hold true, since most mature OSNs express only one olfactory receptor (75%), with 14% expressing 2 and $<1\%$ expressing 3 (Fig. 3b). Cells with two olfactory receptors did not express more unique molecular identifiers (UMIs), suggesting that these were not the result of doublets (Extended Data Fig. 7b). While we have carefully considered the number of genes and UMIs, it is important to consider other potential technical issues with this approach. For instance, one cannot completely exclude the possibility of a doublet from two low-quality libraries having a similar number of genes as a true single cell. Nonetheless, our data are consistent with singular olfactory receptor expression in most cells captured in this study. We found 8 olfactory receptors expressed in more cells than statistically expected, with olfactory receptor 10A6 being the most frequent olfactory receptor, expressed in 5% of olfactory receptor-expressing neurons (Fig. 3c). Both, class I and class II olfactory receptors were identified (Fig. 3d). Six olfactory receptors were statistically more coexpressed than others (Fig. 3e,f and Supplementary Table 9). We found similarities to murine olfactory neurons in terms of the high expression of nonolfactory receptor G protein-coupled receptors (GPCRs), including adiponectin receptor 1, D(2) dopamine receptor, transmembrane protein 181, adhesion G protein-coupled receptor L3 and G protein-coupled receptor family C group 5 member C, the latter encoding a retinoic acid-inducible GPCR (Supplementary Table 10). D(2) dopamine receptor was highly neuron-specific, whereas the other nonolfactory receptor GPCRs were also expressed in nonneuronal clusters. While we did not find other vomeronasal-1 receptors or trace amino acid receptors, we cannot exclude their expression by cells not captured in our biopsies.

Our findings provide direct evidence for ongoing robust neurogenesis in adult olfactory neuroepithelia in humans. The presence and quantification of individual cell populations expressing features defining various stages from stem cell to progenitor cell, and immature to mature neuron are clearly defined at single-cell resolution. In this study, we identify a high ratio of immature to mature neurons in the olfactory neuroepithelium of middle-aged humans, which contrasts the typical populations present in adult rodents. In addition, we define a large set of olfactory receptors that appear to be expressed in the human olfactory neuroepithelium and provide support for singular olfactory receptor expression in mature olfactory neurons. Together, these results provide detailed insights into olfactory neurogenesis in the adult human.

Online content

Any methods, additional references, Nature Research reporting summaries, source data, extended data, supplementary information,

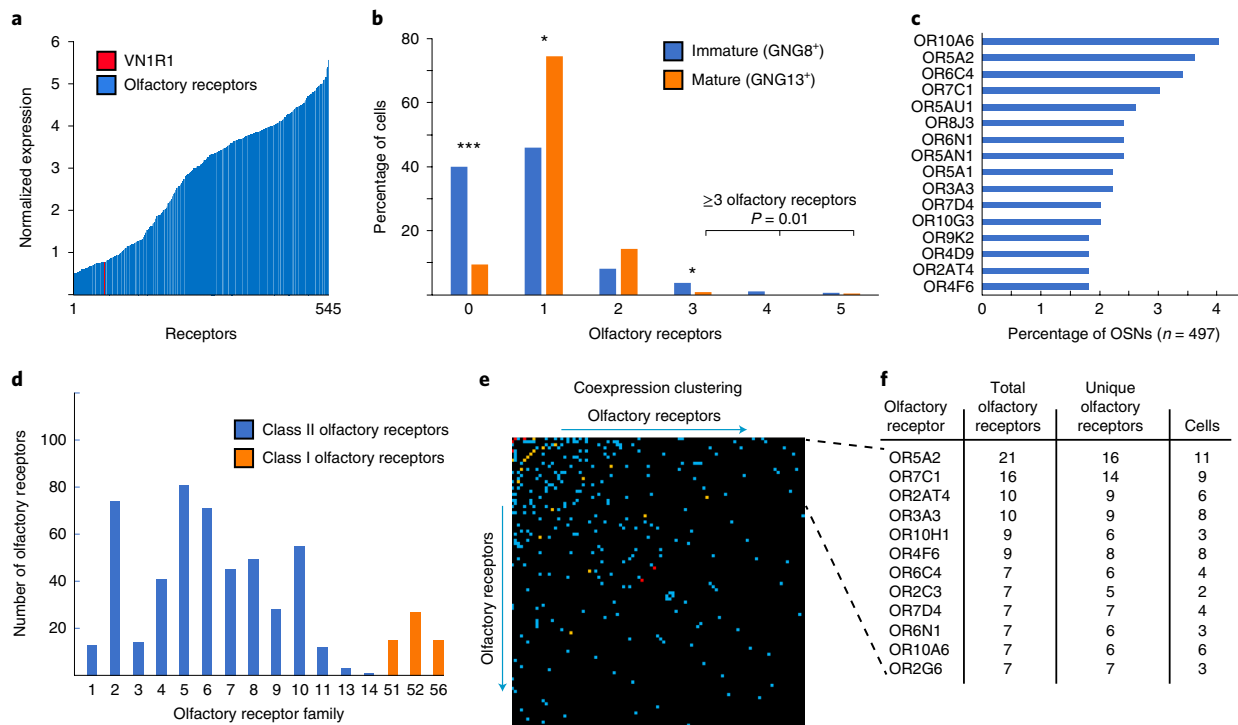


Fig. 3 | Analysis of olfactory receptor expression in human olfactory epithelium. **a**, Expression levels of all olfactory receptors ($n=545$ total receptors) in immature (GNG8⁺) and mature (GNG13⁺) OSNs. Expression levels of a VN1R1 receptor in one cell is indicated in red. The y axis represents normalized expression values; the x axis represents individually expressed receptors. **b**, Olfactory receptors expressed in individual immature and mature neurons. The y axis represents the percentage of the cell population; the x axis represents the number of unique olfactory receptors per cell. * $P < 0.05$; ** $P < 0.001$, two-sided χ^2 test without Yates's correction, $n=3$ patients. The y axis represents the percentage of OSNs ($n=497$). **c**, Most commonly identified olfactory receptors in OSNs. The top eight olfactory receptors in this list were detected statistically more than expected. **d**, Expression of olfactory receptor families in immature and mature neurons; blue, class II, orange, class I olfactory receptors. **e**, Coexpression matrix of olfactory receptors; the x and y axes contain every olfactory receptor found to be coexpressed with at least one other olfactory receptor ($n=141$, including VN1R1). The blue squares show the expression of intersecting olfactory receptors coexpressed in one cell; orange indicates two cells and red three cells. **f**, List of most coexpressed olfactory receptors from **e**. ‘Total olfactory receptors’ indicates the sum of all olfactory receptors found coexpressed with the indicated member; ‘unique olfactory receptors’ indicates the sum of unique olfactory receptor genes coexpressed in the indicated number of neuronal cells. The top six olfactory receptors in this list are statistically more coexpressed than expected.

acknowledgements, peer review information; details of author contributions and competing interests; and statements of data and code availability are available at <https://doi.org/10.1038/s41593-020-0587-9>.

Received: 24 May 2019; Accepted: 3 January 2020;

Published online: 17 February 2020

References

- Hinds, J. W., Hinds, P. L. & McNelly, N. A. An autoradiographic study of the mouse olfactory epithelium: evidence for long-lived receptors. *Anat. Rec.* **210**, 375–383 (1984).
- Schwob, J. E., Szumowski, K. E. & Stasky, A. A. Olfactory sensory neurons are tropically dependent on the olfactory bulb for their prolonged survival. *J. Neurosci.* **12**, 3896–3919 (1992).
- Leung, C. T., Coulombe, P. A. & Reed, R. R. Contribution of olfactory neural stem cells to tissue maintenance and regeneration. *Nat. Neurosci.* **10**, 720–726 (2007).
- Goldstein, B. J. et al. Adult c-Kit⁺ progenitor cells are necessary for maintenance and regeneration of olfactory neurons. *J. Comp. Neurol.* **523**, 15–31 (2015).
- Fletcher, R. B. et al. Deconstructing olfactory stem cell trajectories at single-cell resolution. *Cell Stem Cell* **20**, 817–830.e8 (2017).
- Brann, J. H. & Firestein, S. J. A lifetime of neurogenesis in the olfactory system. *Front. Neurosci.* **8**, 182 (2014).
- Hahn, C. G. et al. In vivo and in vitro neurogenesis in human olfactory epithelium. *J. Comp. Neurol.* **483**, 154–163 (2005).
- Holbrook, E. H., Wu, E., Curry, W. T., Lin, D. T. & Schwob, J. E. Immunohistochemical characterization of human olfactory tissue. *Laryngoscope* **121**, 1687–1701 (2011).
- Graziadei, P. P., Karlan, M. S., Graziadei, G. A. & Bernstein, J. J. Neurogenesis of sensory neurons in the primate olfactory system after section of the fila olfactoria. *Brain Res.* **186**, 289–300 (1980).
- Becht, E. et al. Dimensionality reduction for visualizing single-cell data using UMAP. *Nat. Biotechnol.* **37**, 38–44 (2019).
- van der Maaten, L. & Hinton, G. Visualizing data using t-SNE. *J. Mach. Learn. Res.* **9**, 2579–2605 (2008).
- Corada, M. et al. Sox17 is indispensable for acquisition and maintenance of arterial identity. *Nat. Commun.* **4**, 2609 (2013).
- Chen, M., Reed, R. R. & Lane, A. P. Acute inflammation regulates neuroregeneration through the NF-κB pathway in olfactory epithelium. *Proc. Natl Acad. Sci. USA* **114**, 8089–8094 (2017).
- Schwob, J. E., Youngentob, S. L. & Mezza, R. C. Reconstitution of the rat olfactory epithelium after methyl bromide-induced lesion. *J. Comp. Neurol.* **359**, 15–37 (1995).
- Monahan, K., Horta, A. & Lomvardas, S. LHX2- and LDB1-mediated trans interactions regulate olfactory receptor choice. *Nature* **565**, 448–453 (2019).
- Hirota, J. & Mombaerts, P. The LIM-homeodomain protein Lhx2 is required for complete development of mouse olfactory sensory neurons. *Proc. Natl Acad. Sci. USA* **101**, 8751–8755 (2004).
- Wallrabenstein, I. et al. The smelling of Hedione results in sex-differentiated human brain activity. *Neuroimage* **113**, 365–373 (2015).
- Lyons, D. B. et al. An epigenetic trap stabilizes singular olfactory receptor expression. *Cell* **154**, 325–336 (2013).
- Buck, L. & Axel, R. A novel multigene family may encode odorant receptors: a molecular basis for odor recognition. *Cell* **65**, 175–187 (1991).
- Chess, A., Simon, I., Cedar, H. & Axel, R. Allelic inactivation regulates olfactory receptor gene expression. *Cell* **78**, 823–834 (1994).

Publisher's note Springer Nature remains neutral with regard to jurisdictional claims in published maps and institutional affiliations.

© The Author(s), under exclusive licence to Springer Nature America, Inc. 2020

Methods

Patients and sample collection. Human tissue samples were obtained with patient written informed consent and with approval of the institutional review board of the University of Miami. No statistical methods were used to predetermine sample sizes. Data collection and analysis were not performed blind to the conditions of the experiments. Samples for scRNA-seq were randomly selected since patients presented for routine clinical care. Tissue was obtained from patients undergoing transnasal endoscopic surgery to access the pituitary or anterior skull base (Supplementary Table 1). Mucosa was carefully excised from portions of the olfactory cleft along the superior nasal septum or adjacent superior medial vertical lamella of the superior turbinate, uninvolvin with any pathology. Immediately after removal, samples were held on ice in Hank's Balanced Salt Solution and transported to the laboratory. Under a dissecting microscope, any bone or deep stroma was trimmed away from the epithelium and underlying lamina propria. A small portion of the specimen was sharply trimmed and snap-frozen in optimal cutting temperature medium, to be cryosectioned for histology use. The remaining specimen was then enzymatically dissociated using collagenase type I, dispase and DNase for approximately 30 min. Next, papain was added for 10 min, followed by 0.125% trypsin for 3 min. Cells were filtered through a 100 µm strainer, pelleted and washed and then treated with an erythrocyte lysis buffer and washed again. The cells were then resuspended in PBS with 0.1% bovine serum albumin and immediately processed for scRNA-seq using the Chromium (10X Genomics) platform. Fresh human tissue samples used to generate scRNA-seq data were exhausted in the experimental process.

scRNA-seq. scRNA-seq was performed using the Chromium (10X Genomics) platform. Single-cell suspensions were counted using both the Cellometer K2 Fluorescent Viability Cell Counter (Nexcelom Bioscience) and a hemocytometer, ensuring >80% viability, and adjusted to 1,000 cells µl⁻¹. Samples 1 and 3 were run using the Chromium Single Cell 3' Library & Gel Bead Kit v2 (10X Genomics) and samples 2 and 4 were run using the Chromium Single Cell 3' Library & Gel Bead Kit v3 (10X Genomics). The manufacturer's protocol was used with a target capture of 10,000 cells for the 3' gene expression samples. Each sample was processed on an independent Chromium Single Cell A Chip (10X Genomics) and subsequently run on a thermocycler (Eppendorf); 3' gene expression libraries were sequenced using the NextSeq 500 (Illumina) high output flow cells.

scRNA-seq analysis. Raw base call files were analyzed using Cell Ranger v.3.0.2. The 'mkfastq' command was used to generate FASTQ files and the 'count' command was used to generate raw gene-barcode matrices aligned to the GRCh38 Ensembl 93 genome. The data from all 4 samples was combined in R v.3.5.2 using the Seurat package v.3.0.0 and an aggregate Seurat object was generated^{21,22}. To ensure our analysis was on high-quality cells, filtering was conducted by retaining cells that had UMIs >400, expressed 100–8,000 genes inclusive and had mitochondrial content <10%. This resulted in a total of 28,726 cells. Data for all four samples were combined using the standard integration workflow (<https://satijalab.org/seurat/v3.0/integration.html>). Data from each sample were normalized using the NormalizeData() function and variable features were identified using FindVariableFeatures() with 5,000 genes; the selection method was set to 'vst', a variance stabilizing transformation. To identify the integration of anchor genes among the 4 samples, the FindIntegrationAnchors() function was used with 30 principal components and 5,000 genes. Using Seurat's IntegrateData(), samples were combined into one object. Data were scaled using the ScaleData() function to reduce the dimensionality of this dataset; principal component analysis was used, and the first 30 principal components were summarized further using UMAP dimensionality reduction²³. We chose to use 30 principal components based on the results from the analysis using JackStraw and elbow plots (Extended Data Fig. 8a,b). The DimPlot() function was used to generate the UMAP plots displayed. Clustering was conducted using the FindNeighbors() and FindClusters() functions using 30 principal component analysis components and a resolution parameter set to 1.8. The original Louvain algorithm was used for modularity optimization²⁴. The resulting 26 Louvain clusters were visualized in a two-dimensional UMAP representation and were annotated to known biological cell types using canonical marker genes, as well as gene set enrichment analysis (enrichR v.2.1) (ref. ²⁵). Quality control plots depict UMI and gene distributions per cluster (Extended Data Fig. 9). The list of top significant genes for each cluster was inputted into the enrichR tool; Gene Ontology, cellular pathway and tissue output terms were used to help verify that cell phenotype assignments were consistent with these outputs. The following cell types were annotated (selected markers are listed): CD8⁺ T Cells (*CD3D*, *CD3E*, *CD8A*); CD4⁺ T Cells (*CD3D*, *CD3E*, *CD4*, *IL7R*); natural killer cells (*FGFBP2*, *FCGR3A*, *CX3CR1*); B cells (*CD19*, *CD79A*, *MS4A4A*); plasma cells (*MZB1*, *SDC1*, *CD79A*); monocytes (*CD14*, *S100A12*, *CLEC10A*); macrophages (*C1QA*, *C1QB*, *C1QC*); dendritic cells (*CD1C* and lack of expression of *C1QA*, *C1QB* and *C1QC*); mast cells (*TPSB2*, *TPSAB1*); fibroblasts/stromal cells (*LUM*, *DCN*, *CLEC11A*); respiratory ciliated cells (*FOXJ1*, *CFAP126*, *STOML3*); respiratory HBCs (*KRT5*, *TP63*, *SOX2*); respiratory gland progenitor cells (*SOX9*, *SCGB1A1*); respiratory secretory cells (*MUC5*, *CYP4B1*, *TFF3*); vascular smooth muscle cells (*TAGLN*, *MYH11*); pericytes (*SOX17*, *ENG*); Bowman's glands (*SOX9*, *SOX10*, *MUC5*, *GPX3*); olfactory HBCs (*TP63*, *KRT5*, *CXCL14*, *SOX2*, *MEG3*).

olfactory ensheathing glia (*S100B*, *PLP1*, *PMP2*, *MPZ*, *ALX3*); olfactory microvillar cells (*ASCL3*, *CFTR*, *HEPACAM2*, *FOXL1*); immature neurons (*GNG8*, *OLIG2*, *EBF2*, *LHX2*, *CBX8*); mature neurons (*GNG13*, *EBF2*, *CBX8*, *RTP1*); GBCs (*HES6*, *ASCL1*, *CXCR4*, *SOX2*, *EZH2*, *NEUROD1*, *NEUROG1*); and sustentacular cells (*CYP2A13*, *CYP2J2*, *GPX6*, *ERMN*, *SOX2*). To generate a heatmap (Fig. 1) of the cell types of interest (Bowman's glands, olfactory HBCs, olfactory microvillar cells, immature and mature neurons, GBCs and sustentacular cells), the Seurat subset() function was used followed by the AverageExpression() function to generate average RNA expression data for each cell type. Hierarchical clustering was conducted on the RNA-averaged clusters with genes aggregated from the literature and visualized using ComplexHeatmap v.1.20.0 (ref. ²⁶). Subanalysis to count cells expressing GPCRs and other genes (Fig. 3) was done by extracting cells from the olfactory neuronal lineage clusters expressing *GNG8* or *GNG13*, which includes some GBCs/nascent neurons, and immature and mature neurons. For samples from patient 2 and 3, the proportion of GBCs in the olfactory neuroepithelium was calculated based on the total number of olfactory neuroepithelium phenotypes per sample (HBCs, GBCs, immature OSNs, mature OSNs, microvillar cells and sustentacular cells).

Single-cell neuron subpopulation analysis. For the analysis, we used the normalized expression data from the 'GBCs', 'immature neurons' and 'mature neurons' subsets to infer the relationship between these cell types. The subset() command was used with the option 'do.clean' set to 'TRUE'. A new analysis on this subset was performed on the neuronal subset using the FindVariableFeatures(), ScaleData(), RunPCA() and RunUMAP() functions. New UMAP plots were generated for this subpopulation (Fig. 1e), along with feature plots for specific gene expression visualization (Fig. 2f). In addition, DotPlots, where the size of the circle indicates the percentage of cells in a cluster expressing the marker and the color indicates expression level, were generated to further visualize gene expression data, using the DotPlot function in Seurat (Fig. 2a and Extended Data Figs. 1, 4 and 5). Subanalysis to count cells expressing GPCRs and other genes (Fig. 3) was done by extracting cells from the olfactory neuronal lineage clusters. A cutoff of 0.5 normalized expression counts, as determined by Seurat ($\log(\text{reads} \times 10,000 / \text{total reads})$), was applied (Extended Data Fig. 7a); this excluded approximately 15% of all data (considered low expression). Furthermore, 0.5 is around 10% of the maximum expression detected; there are few observations >5 normalized expression values. Of note, >75% of olfactory receptors we report have an expression value >1 and >50% have an expression value >2. While there is no clear guidance on which cutoffs are standard for scRNA-seq data, we regard our choice for reporting olfactory receptor expression as stringent.

Statistical significance was calculated with the two-sided χ^2 test without Yates's correction, using RStudio v.1.0.143 and R v.3.4.0 with the chisq.test() function. Other analyses were performed using custom-coded Python scripts (Supplementary Software; https://github.com/harbourlab/OR_SC_analysis). For olfactory receptor coexpression, an outlier test was performed assuming that the data range should fall within $Q3 + 1.5 \times \text{interquartile range (IQR)}$, with $Q3$ being the 75th percentile of the data and $\text{IQR} = Q3 - Q1$, $Q1$ being the 25th percentile (Fig. 3). Neurons expressing >1 olfactory receptor did not express significantly more genes, nor were significantly more UMIs detected (Extended Data Fig. 7b). UMIs are the number of UMIs sequenced (number of unique transcripts). The UMI count is expected to double in bona fide doublets of similar cells due to the stochastic sequencing nature of the mixed library. While our findings generally support singular olfactory receptor expression by olfactory neurons along with occasional cells expressing >1 olfactory receptor, it is important to note that there are other technical issues making it difficult to definitively exclude the possibility of multiple cells erroneously being considered as a single cell.

Gene set enrichment analysis. The FindMarkers() function was used to conduct differential gene expression analysis between annotated clusters of interest. The 'fgsea' package v1.8.0 was used²⁷ with default settings from the Reactome pathway vignette with the 'reactome.db' package²⁸ v1.68.0 providing curated pathways from Reactome²⁹ v68. The top 50 pathways ranked by adjusted *P* value were plotted in the visualization (Extended Data Fig. 6).

IHC. Cryosections were prepared from nasal epithelium biopsies. Tissue was embedded in optimal cutting temperature medium and snap-frozen in liquid nitrogen, or was first fixed in 4% paraformaldehyde for 3 h, rinsed in PBS, cryoprotected in 30% sucrose in PBS and then embedded and frozen. Sections 10-µm thick were prepared using a Leica CM1850 cryostat (Leica Biosystems) and mounted onto SuperFrost Plus adhesion slides (VWR) and stored at -20°C. Sections were fixed with 4% paraformaldehyde in phosphate buffer (if not previously fixed), rinsed in PBS and processed for IHC. After treatment with an ethanol gradient (70, 95, 100, 95, 70%), PBS rinse and any required pretreatments, tissue sections were incubated in blocking solution with 10% donkey serum, 5% bovine serum albumin, 4% nonfat dry milk and 0.1% Triton X-100 for 30 min at room temperature. Primary antibodies (Supplementary Table 11) were diluted in this same solution and incubated overnight in a humidified chamber at 4°C.

Detection by species-specific fluorescent conjugated secondary antibodies, validated for multilabeling, was performed at room temperature for 45 min.

Sections were counterstained with 4,6-diamidino-2-phenylindole (DAPI) and coverslips were mounted using ProLong Gold Antifade Mountant (Thermo Fisher Scientific) for imaging, using a Leica DMI8 microscope system (Leica Microsystems). Images were processed using the ImageJ software v.2.0.0-rc-69/1.52p (NIH). Scale bars were applied directly from the Leica acquisition software metadata in ImageJ Tools. Adult C57BL/6 (The Jackson Laboratory) mouse cryosections were prepared as described previously³⁰ and immunostained in parallel with the human sections. Animal work was approved by the Institutional Animal Care and Use Committee, University of Miami. Immunostaining for mouse tissue was performed on three independent mouse replicates for TUJ1, KRT5 and LHX2, and five independent mouse replicates for KI67. For quantification (Fig. 2), we used human samples containing intact olfactory neuroepithelium, rather than respiratory epithelium, with enough sections meeting the criteria available from 3 patients (case nos. 5, 6 and 7), and quantified labeling from 20x fields in ≥ 2 sections per patient, using ImageJ. Data distribution was formally tested and found to be normal. For IHC quantification comparisons, the two-sided Welch's *t*-test was used. Blinding was not feasible since human and mouse histology contain obvious differences. No animals or data points were excluded from the analysis.

Statistics. No statistical method was used to predetermine sample size. For each experiment, tissue samples from a single patient were processed individually. Single-cell suspensions for each sample were processed for scRNA-seq (10x Genomics) in an independent Chromium chip. For IHC quantification comparisons, the two-sided Welch's *t*-test was used. For olfactory receptor analysis, statistical significance was calculated with the two-sided χ^2 test without Yates's correction. For differential expression analysis in Seurat, the default two-sided nonparametric Wilcoxon rank-sum test was used with Bonferroni correction using all genes in the dataset.

Reporting Summary. Further information on research design is available in the Nature Research Reporting Summary linked to this article.

Data availability

All sequencing data generated have been deposited with the Gene Expression Omnibus under accession code [GSE139522](#). Source data are provided for Figs. 2 and 3 and Extended Data Figs. 1 and 7.

Code availability

The code used for the olfactory receptor analysis is available at https://github.com/harbourlab/OR_SC_analysis.

References

21. Stuart, T. et al. Comprehensive integration of single-cell data. *Cell* **177**, 1888–1902.e21 (2019).
22. Butler, A., Hoffman, P., Smibert, P., Papalexi, E. & Satija, R. Integrating single-cell transcriptomic data across different conditions, technologies, and species. *Nat. Biotechnol.* **36**, 411–420 (2018).
23. McInnes, L., Healy, J., Saul, N. & Grossberger, L. UMAP: uniform manifold approximation and projection. *J. Open Source Softw.* **3**, 861 (2018).
24. Blondel, V. D., Guillaume, J.-L., Lambiotte, R. & Lefebvre, E. Fast unfolding of communities in large networks. *J. Stat. Mech.* **2008**, P10008 (2008).
25. Kuleshov, M. V. et al. Enrichr: a comprehensive gene set enrichment analysis web server 2016 update. *Nucleic Acids Res.* **44**, W90–W97 (2016).
26. Gu, Z., Eils, R. & Schlesner, M. Complex heatmaps reveal patterns and correlations in multidimensional genomic data. *Bioinformatics* **32**, 2847–2849 (2016).
27. Korotkevich, G., Sukhov, V. & Sergushichev, A. Fast gene set enrichment analysis. Preprint at *bioRxiv* <https://doi.org/10.1101/060012> (2019).
28. Ligtenberg, W. reactome.db: a set of annotation maps for reactome. R package version 1.68.0 <http://bioconductor.org/packages/release/data/annotation/html/reactome.db.html> (2019).
29. Fabregat, A. et al. The Reactome Pathway Knowledgebase. *Nucleic Acids Res.* **46**, D649–D655 (2018).
30. Goldstein, B. J. et al. Contribution of Polycomb group proteins to olfactory basal stem cell self-renewal in a novel c-KIT⁺ culture model and in vivo. *Development* **143**, 4394–4404 (2016).

Acknowledgements

We are grateful to the patients who generously contributed samples for this research. We acknowledge the assistance of the Onco-Genomics Shared Resource at the Sylvester Comprehensive Cancer Center and the University of Miami Center for Computational Science. This work was supported by funding from National Institutes of Health grant nos. DC013556 (B.J.G), DC016859 (B.J.G) and CA125970 (J.W.H.), the Triological Society/American College of Surgeons (B.J.G.), the University of Miami Sheila and David Fuente Graduate Program in Cancer Biology (M.A.D.) and the Center for Computational Science Fellowship (M.A.D.). The Sylvester Comprehensive Cancer Center also received funding from the National Cancer Institute Core Support Grant no. P30CA240139.

Author contributions

M.A.D. and Stefan Kurtenbach analyzed and interpreted the data and wrote the manuscript. B.J.G. designed and led the project, performed the experiments, interpreted the data and wrote the manuscript. Z.B.S. provided the clinical samples and interpreted the data. J.W.H. designed the experiments and interpreted the data. R.C., G.M.G and Sarah Kurtenbach performed the experiments and interpreted the data. H.M. interpreted the data and edited the manuscript.

Competing interests

J.W.H. is the inventor of intellectual property related to prognostic testing for uveal melanoma. He is a paid consultant for Castle Biosciences, a licensee of this intellectual property and receives royalties from its commercialization. The other authors do not have any potential competing interests.

Additional information

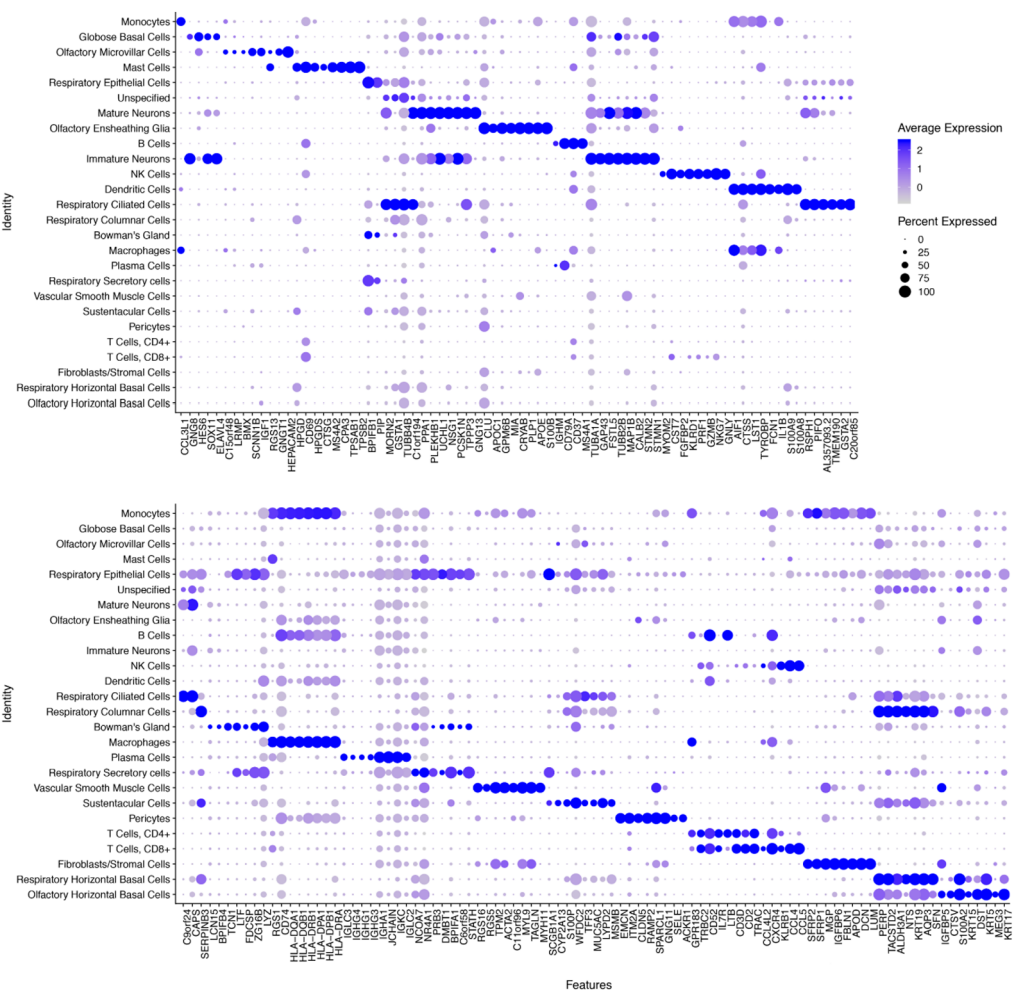
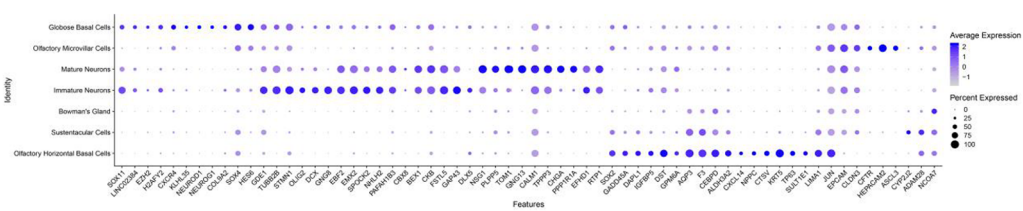
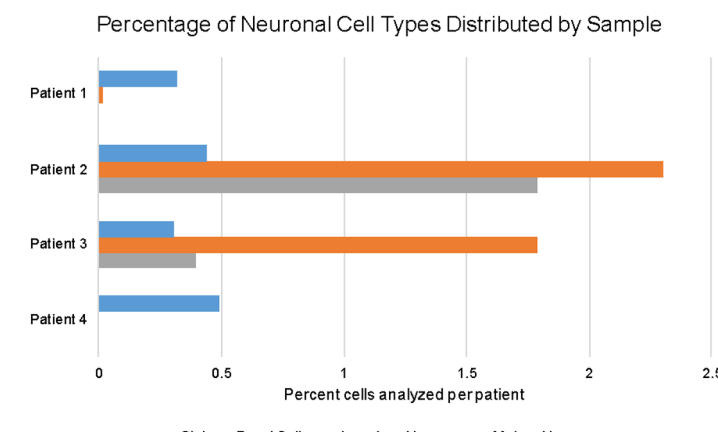
Extended data is available for this paper at <https://doi.org/10.1038/s41593-020-0587-9>.

Supplementary information is available for this paper at <https://doi.org/10.1038/s41593-020-0587-9>.

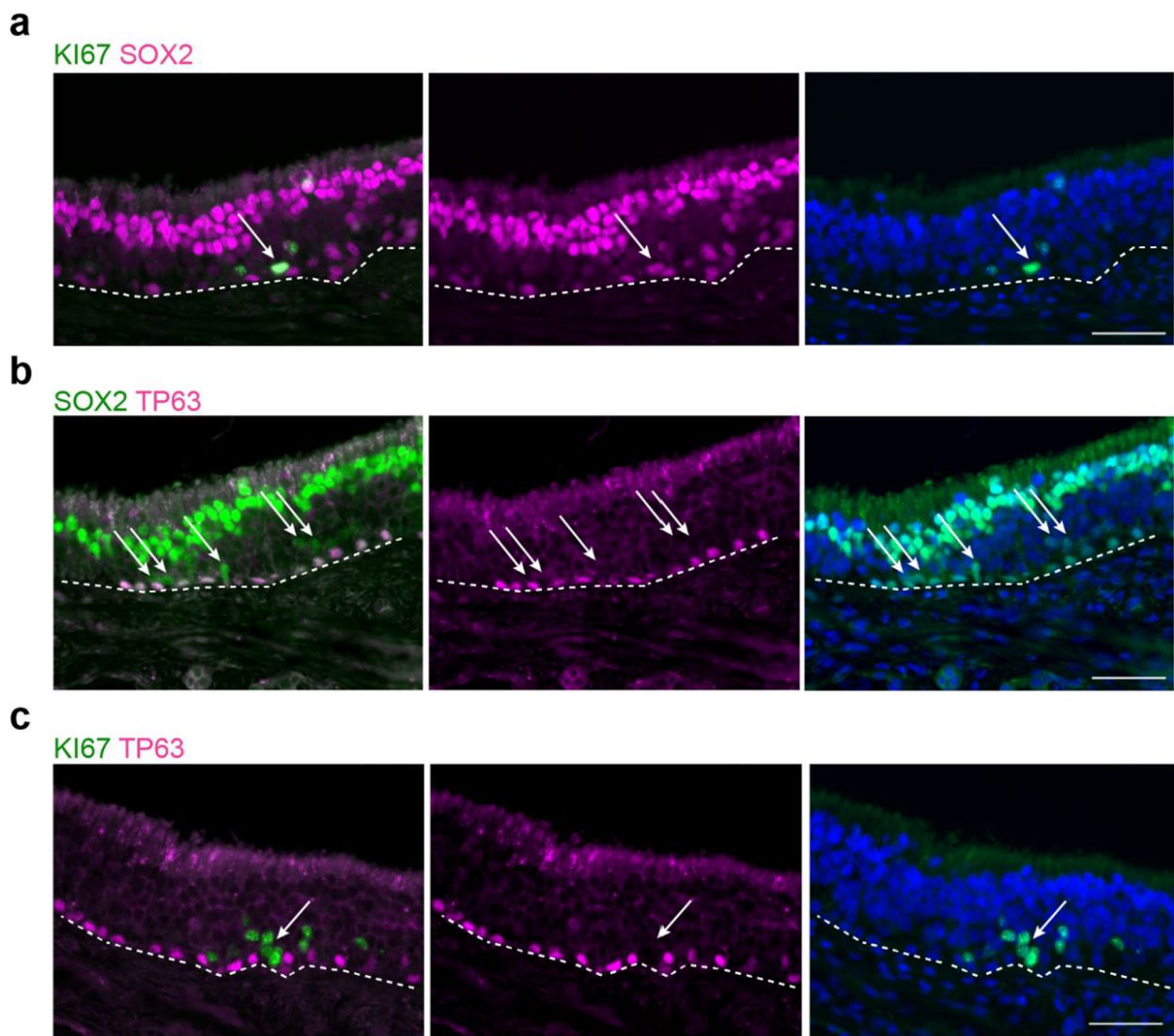
Correspondence and requests for materials should be addressed to B.J.G.

Peer review information *Nature Neuroscience* thanks Thomas Berger, Sandrine Thuret and the other, anonymous, reviewer(s) for their contribution to the peer review of this work.

Reprints and permissions information is available at www.nature.com/reprints.

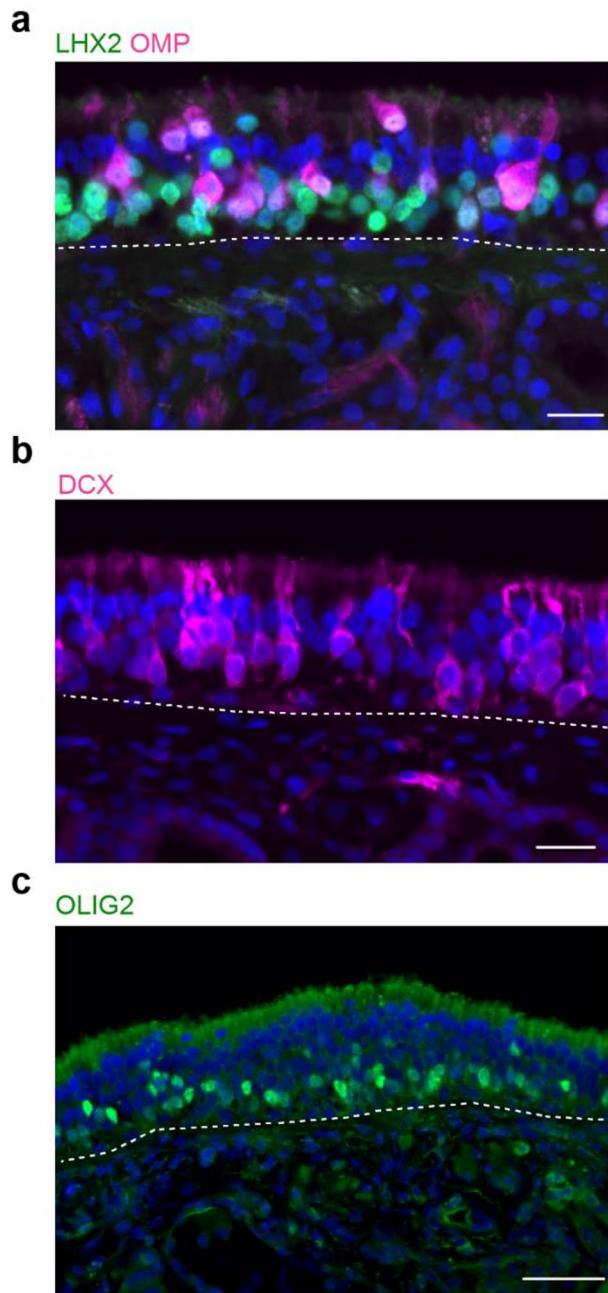
a**b****c****Extended Data Fig. 1 | See next page for caption.**

Extended Data Fig. 1 | DotPlot visualization listing scRNA-seq clusters. **a**, Cell phenotypes listed on y-axis, showing unbiased gene expression for the top 8 genes per cluster identified by log Fold Change; genes (features) are listed along the x-axis. Dot size reflects percentage of cells in a cluster expressing each gene; dot color reflects expression level (as indicated on legend). The plot depicts clusters from 28,726 combined olfactory and respiratory mucosal cells, n=4 patients. **b**, DotPlot visualization of the Heatmap shown in Fig. 1d. The plot depicts clusters from 28,726 combined olfactory and respiratory mucosal cells, n=4 patients. **c**, Histogram showing the neuronal lineage cell types captured by scRNA-seq, as a percentage of the total cells analyzed per patient; see Fig. 1c.

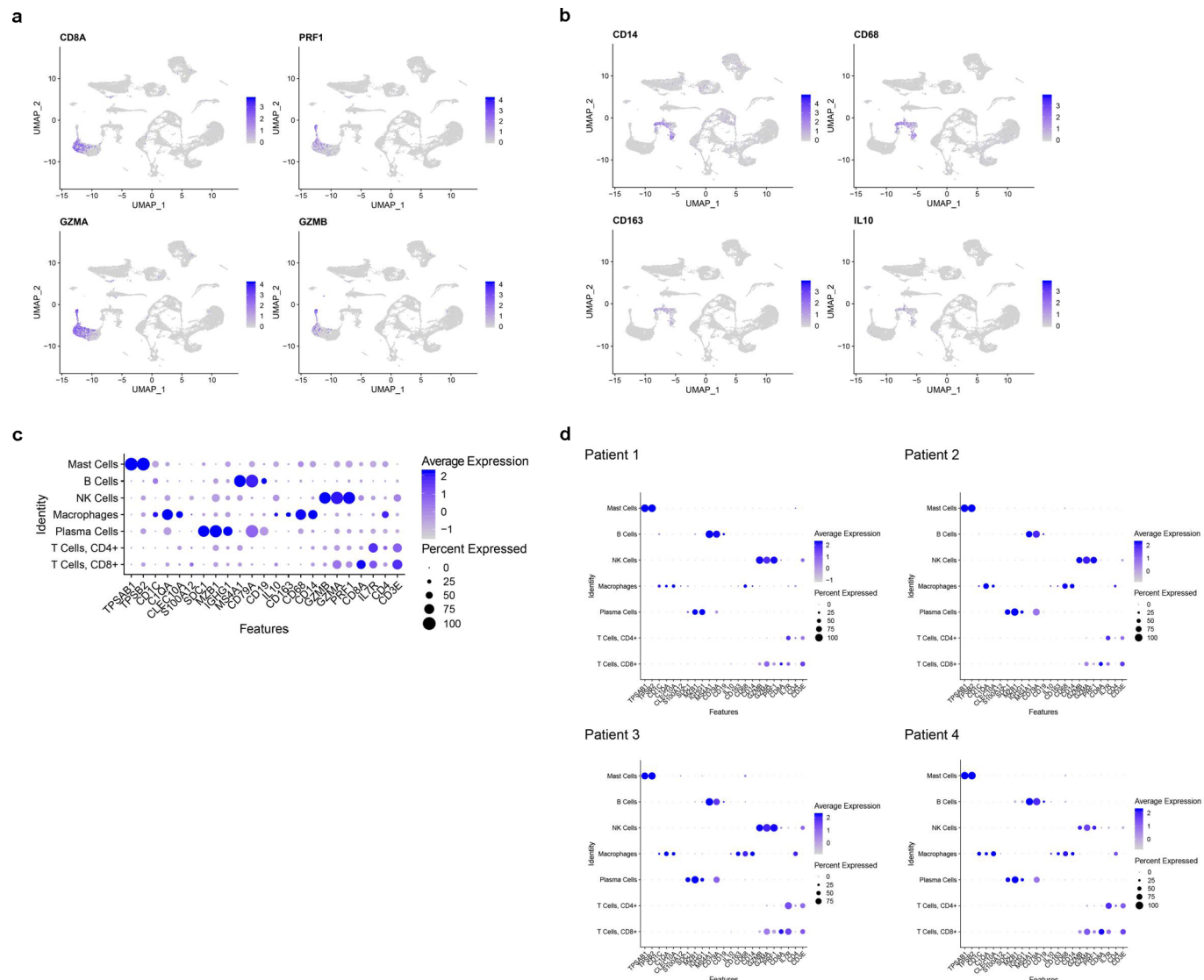


Extended Data Fig. 2 | Additional human immunohistochemistry of basal cell populations. Co-staining for SOX2, Ki67 or the HBC marker TP63.

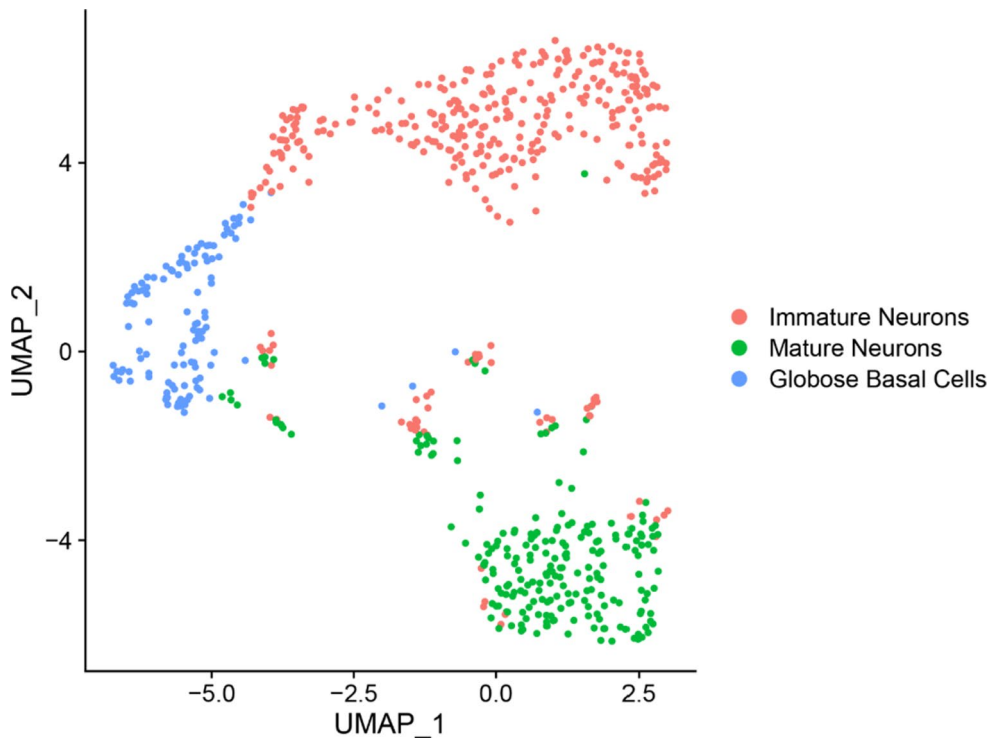
Proliferative activity has been used as a hallmark of the globose basal cell (GBC) phenotype. We reasoned that, although some proliferating cells in the olfactory epithelium (OE) might be immune or inflammatory cells, proliferating cells within the GBC layers of the OE that are SOX2⁺/Ki67⁺/TP63⁺ would be categorized as GBCs. **a**, Sustentacular cell nuclei at the top of the OE are SOX2-bright; and horizontal basal cells (HBCs) and a subset of GBCs are SOX2⁺, although less intensely. Arrow marks a SOX2⁺/Ki67⁺ cell among the proliferative Ki67⁺ basal region, consistent with the GBC phenotype. **b**, SOX2 co-localizes with TP63 in HBCs; arrows mark Sox2⁺/TP63⁺ GBCs. **c**, TP63⁺ HBCs are mitotically quiescent, while many GBCs are actively proliferating, often in scattered cell clusters. Arrow marks a cluster of KI67⁺/TP63⁺ basal cells. Dashed line indicates basal lamina. Immunostaining for **a-c** was conducted in triplicate with similar results. Scale bar, 50 µm.

**Extended Data Fig. 3 | Additional human immunohistochemistry (IHC) of immature and mature olfactory sensory neurons (OSN) populations.**

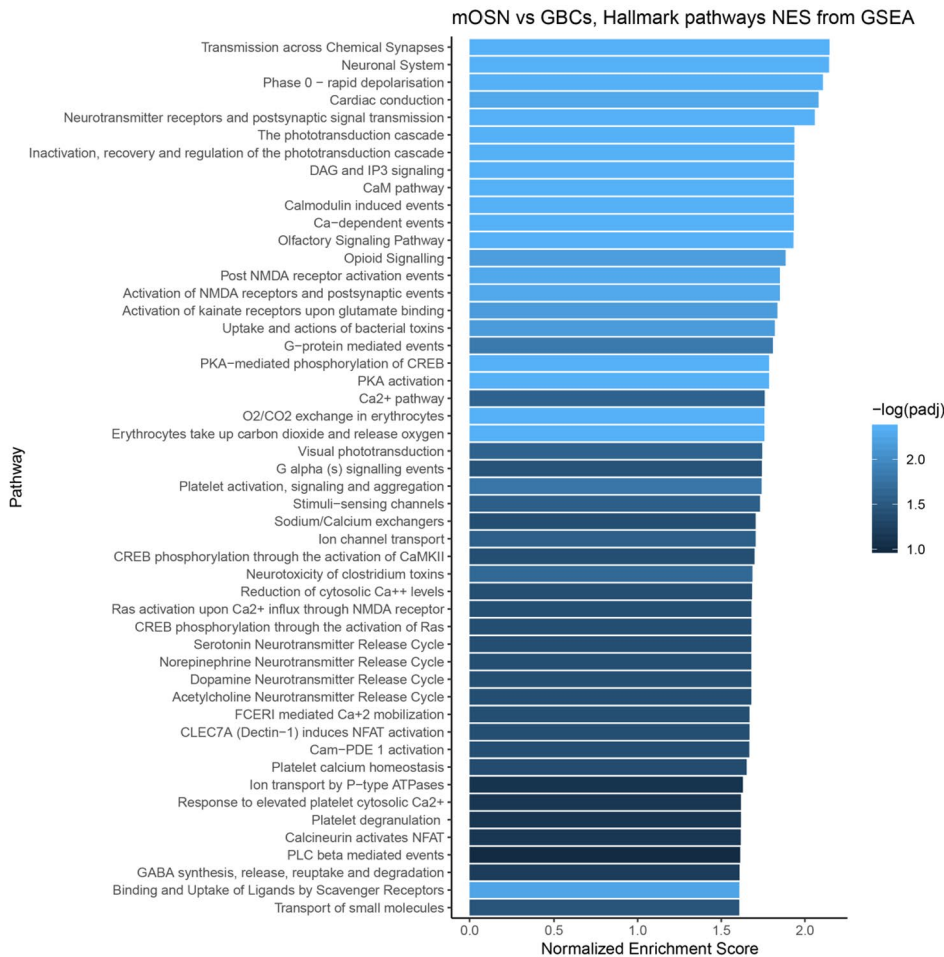
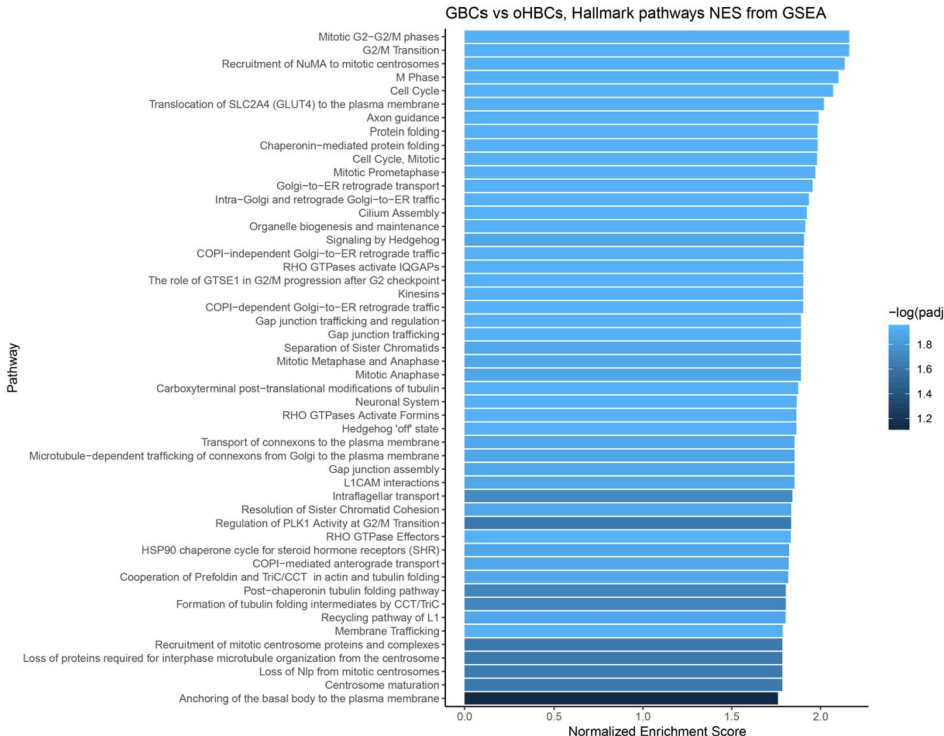
a, Co-staining for LHX2 and OMP demonstrates many LHX2⁺/OMP⁻ neurons, distributed in deeper layers of the OE, which are immature OSNs; OMP is a marker for fully differentiated OSNs, while LHX2 expression in differentiating OSNs orchestrates OR receptor expression. **b**, DCX was identified by scRNA-seq here as enriched in immature OSNs (see Fig. 2a). IHC confirms scattered DCX⁺ neuronal somata and dendrites in the OE. **c**, Similarly, the bHLH transcription factor OLIG2 was identified to be enriched in immature OSNs; IHC confirms nuclear expression in the deeper OSN layers of OE tissue. Dashed line indicates basal lamina. Immunostaining for **a–c** was conducted in triplicate with similar results. Scale bar, 25 μ m.



Extended Data Fig. 4 | Analysis of immune cell populations. Feature plots indicate expression of inflammatory cell markers in human nasal biopsy samples. UMAP clustering identifies lymphocyte populations; **a**, Cytotoxic T cell markers co-localize including CD8A, PRF1, GZMA and GZMB. The plot depicts clusters from 28,726 combined olfactory and respiratory mucosal cells, n = 4 patients. **b**, Within the monocyte/macrophage populations (CD14⁺, CD68⁺ cells), markers for activated M2 macrophages, such as CD163 and IL10, are indicated. The plot depicts clusters from 28,726 combined olfactory and respiratory mucosal cells, n = 4 patients. **c**, DotPlot visualization of additional immune cell gene expression from combined aggregate samples. Cell cluster identity is listed on the y-axis, genes (Features) are listed on x-axis. The plot depicts clusters from 28,726 combined olfactory and respiratory mucosal cells, n = 4 patients. **d**, Immune cell DotPlots showing the contribution of cell types and gene expression patterns by individual patient sample. The plot depicts clusters from 28,726 combined olfactory and respiratory mucosal cells, n = 4 patients.

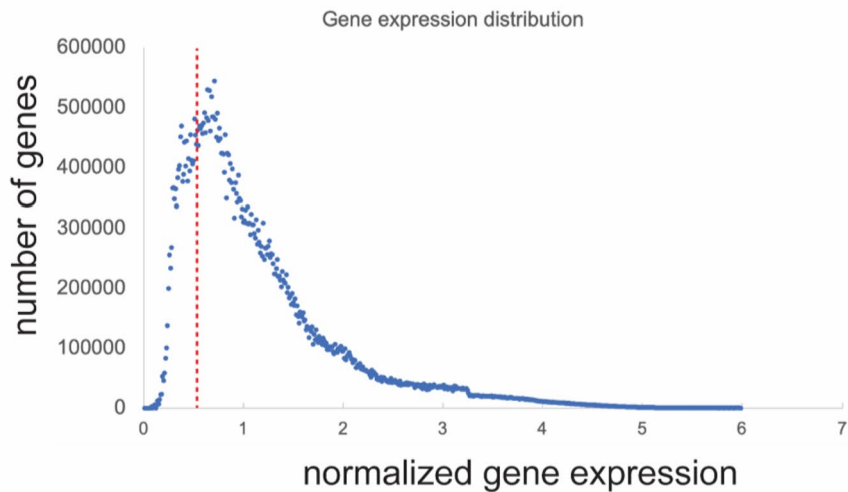
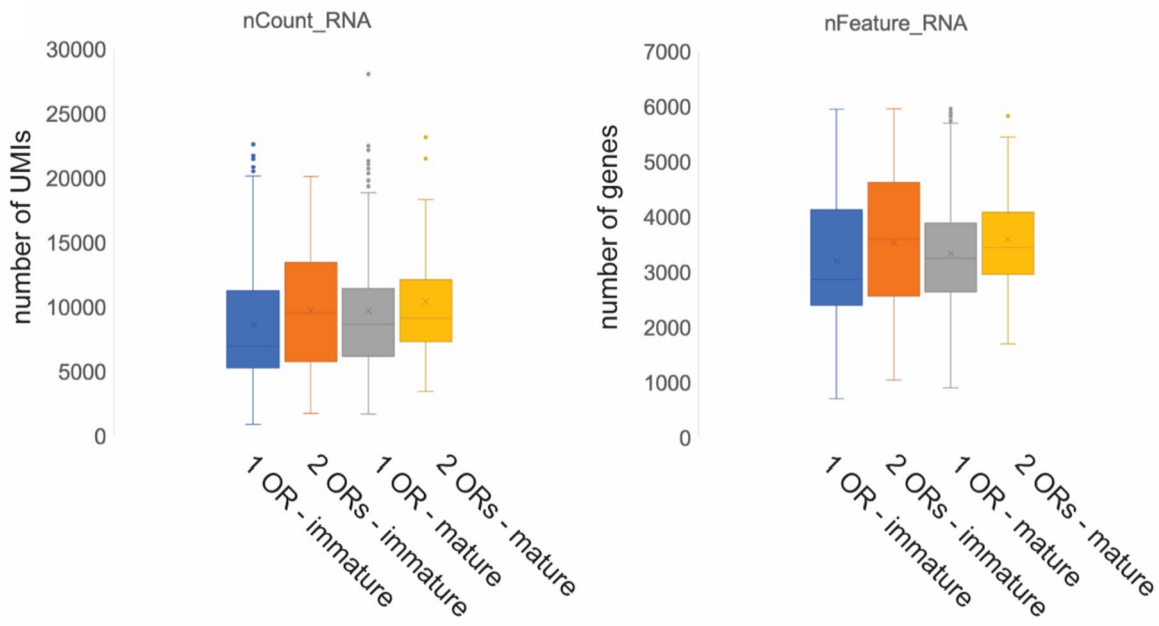


Extended Data Fig. 5 | Focused UMAP plot of OE neuronal lineage populations, with cell phenotype assignments indicated. Compare with gene expression feature plots in Figs. 1e and 2f. The plot depicts clusters from 694 GBCs, immature olfactory neurons and mature olfactory neurons, n=4 patients.

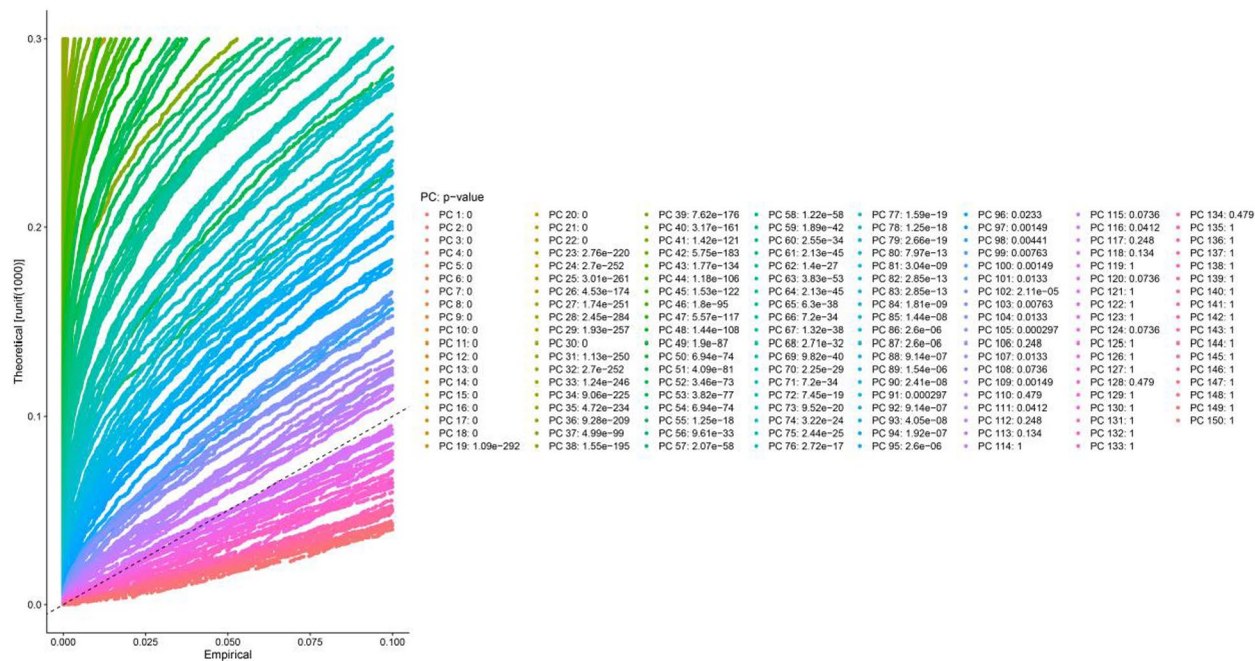
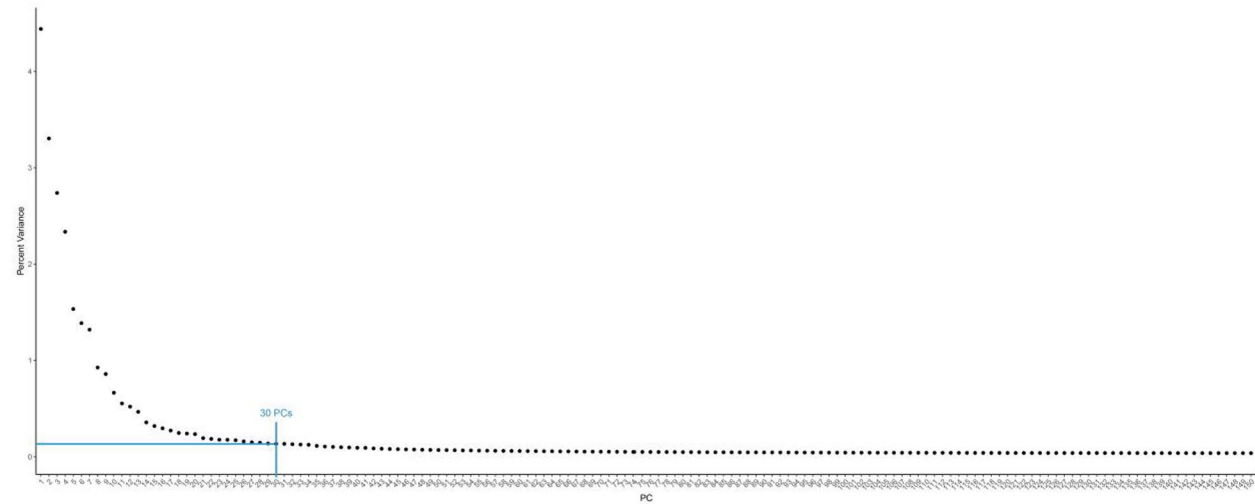
a**b**

Extended Data Fig. 6 | See next page for caption.

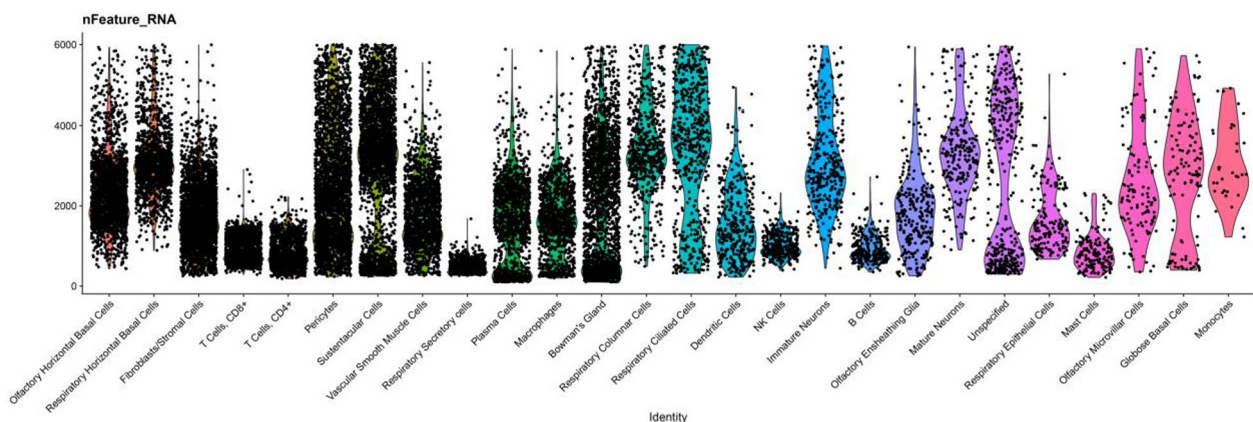
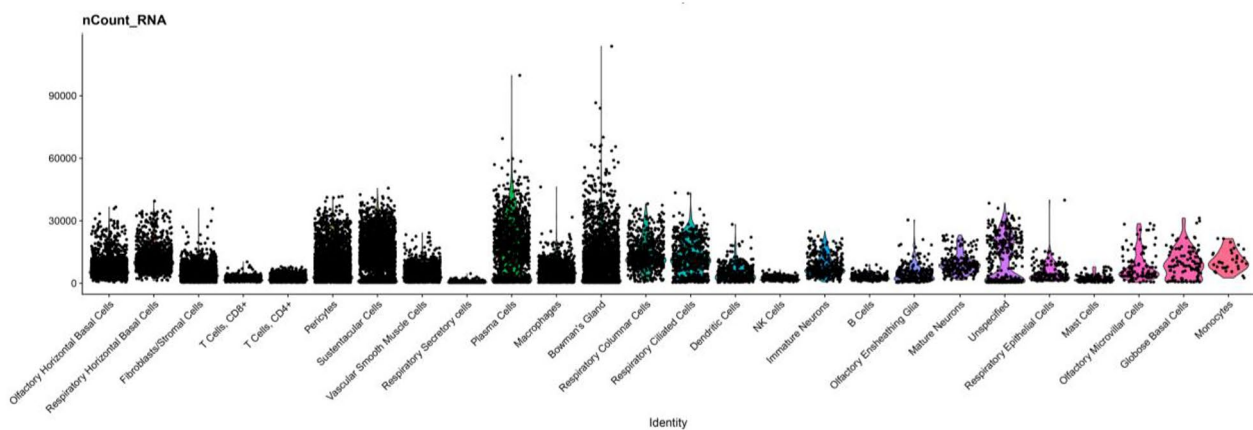
Extended Data Fig. 6 | Gene set enrichment analysis on differential expression data from selected cell clusters. The top 50 Reactome pathways ranked by adjusted P value were plotted in the visualization. **a**, mOSNs versus GBCs; many top terms involve neuronal, transduction and synapse function. The differential expression was calculated in Seurat from 222 mOSNs and 115 GBCs, n=4 patients. The default two-sided enrichment p-value with Benjamini-Hochberg correction from the fgsea package was utilized. **b**, GBCs versus olfactory HBCs; top terms include cell cycle or neurogenesis functions. The differential expression was calculated in Seurat from 115 GBCs and 2,182 olfactory HBCs, n=4 patients. The default two-sided enrichment p-value with Benjamini-Hochberg correction from the fgsea package was utilized.

a**b**

Extended Data Fig. 7 | OR gene expression in human olfactory neurons. **a**, Range of gene expression in our datasets (binned to 0.01). We identified 4.80×10^7 observations (gene expression measurements) expressing > 0 . Genes with no expression ($= 0$, $n = 532063621$) were excluded in this plot. The distribution plot shows that choosing a cutoff of 0.5 (red vertical dotted line). **b**, Doublet analysis. Box plots depicting the number of UMIs (“nCount_RNA”, left plot), and genes (“nFeature_RNA”, right plot) in immature and mature neurons expressing 1 or 2 ORs.

a**b**

Extended Data Fig. 8 | Principal component determination analysis. The 4-patient combined data set was analyzed in Seurat to explore principal components (PCs) contributing to heterogeneity, and to determine an appropriate PC selection. **a**, Using the JackStraw approach, approximately 100 PCs had low a p-value. The plot depicts PC calculated from from 28,726 combined olfactory and respiratory mucosal cells, n=4 patients. The jackstraw test implemented in Seurat was used to calculate p-values of PCs. **b**, To select a suitable number of PCs for downstream analysis, we used the elbow plot heuristic approach, indicating that beyond 20–30 PCs, very little additional variation is explained. Therefore, for downstream analysis we chose to include 30 PCs.

a**b**

Extended Data Fig. 9 | scRNA-seq quality control plots. **a**, Number of genes (nFeature_RNA) per cluster. The plot depicts clusters from 28,726 combined olfactory and respiratory mucosal cells, n=4 patients. **b**, Number of UMIs (nCount_RNA) per cluster. The plot depicts clusters from 28,726 combined olfactory and respiratory mucosal cells, n=4 patients. Cluster cell type identities are listed along the x-axis. Violin plot widths are proportional to the density of the distribution.

Reporting Summary

Nature Research wishes to improve the reproducibility of the work that we publish. This form provides structure for consistency and transparency in reporting. For further information on Nature Research policies, see [Authors & Referees](#) and the [Editorial Policy Checklist](#).

Statistics

For all statistical analyses, confirm that the following items are present in the figure legend, table legend, main text, or Methods section.

n/a Confirmed

- The exact sample size (n) for each experimental group/condition, given as a discrete number and unit of measurement
- A statement on whether measurements were taken from distinct samples or whether the same sample was measured repeatedly
- The statistical test(s) used AND whether they are one- or two-sided
Only common tests should be described solely by name; describe more complex techniques in the Methods section.
- A description of all covariates tested
- A description of any assumptions or corrections, such as tests of normality and adjustment for multiple comparisons
- A full description of the statistical parameters including central tendency (e.g. means) or other basic estimates (e.g. regression coefficient) AND variation (e.g. standard deviation) or associated estimates of uncertainty (e.g. confidence intervals)
- For null hypothesis testing, the test statistic (e.g. F , t , r) with confidence intervals, effect sizes, degrees of freedom and P value noted
Give P values as exact values whenever suitable.
- For Bayesian analysis, information on the choice of priors and Markov chain Monte Carlo settings
- For hierarchical and complex designs, identification of the appropriate level for tests and full reporting of outcomes
- Estimates of effect sizes (e.g. Cohen's d , Pearson's r), indicating how they were calculated

Our web collection on [statistics for biologists](#) contains articles on many of the points above.

Software and code

Policy information about [availability of computer code](#)

Data collection

No software was used for data collection.

Data analysis

General data analysis, statistical tests, and plotting: R 3.5.2 with the packages Seurat (3.0.3), ggplot2 (2.3.2), ComplexHeatmap (1.20.0), dplyr (0.8.3), Rtsne (0.15),forcats (0.3.0), bindrcpp (0.2.2), cowplot (0.9.3), Matrix (1.2-15), scales (1.0.0), jpeg (0.1-8), colorRamps (2.3), paletter (0.0.0.9000), cellranger (1.1.0), IRanges (2.16.0), AnnotationDbi(1.44.0), reactome.db (1.68.0), org.Hs.eg.db (3.7.0), fgsea (1.8.0), EnrichR (2.1).
Image quantification: Fiji ImageJ (vesion 2.0.0-rc-69/1.52p)
Single cell gene expression raw data processing: Cellranger (10X Genomics, version 3.0.2).

For manuscripts utilizing custom algorithms or software that are central to the research but not yet described in published literature, software must be made available to editors/reviewers. We strongly encourage code deposition in a community repository (e.g. GitHub). See the Nature Research [guidelines for submitting code & software](#) for further information.

Data

Policy information about [availability of data](#)

All manuscripts must include a [data availability statement](#). This statement should provide the following information, where applicable:

- Accession codes, unique identifiers, or web links for publicly available datasets
- A list of figures that have associated raw data
- A description of any restrictions on data availability

All sequencing data generated have been deposited in GEO under accession code GSE139522.

Field-specific reporting

Please select the one below that is the best fit for your research. If you are not sure, read the appropriate sections before making your selection.

- Life sciences Behavioural & social sciences Ecological, evolutionary & environmental sciences

For a reference copy of the document with all sections, see nature.com/documents/nr-reporting-summary-flat.pdf

Life sciences study design

All studies must disclose on these points even when the disclosure is negative.

Sample size	No statistical method was used to predetermine sample size. We used fresh human tissue samples obtained from surgical patients. 4 samples underwent scRNAseq and 6 samples underwent IHC.
Data exclusions	No data were excluded.
Replication	scRNA-seq was replicated in 4 individual patient samples. Immunostaining was performed on additional 3 human tissue samples to confirm findings, and compared to mouse tissue staining. Immunostaining for mouse tissue was performed on 3 independent mouse replicates for TUJ1, KRT5, LHX2 and 5 independent mouse replicates for Ki67. All attempts at replication were successful.
Randomization	No randomization was done as there were no treated versus untreated groups; this work involved prospectively collecting tissue for single cell gene expression assays.
Blinding	Blinding was not feasible. For instance, histologic appearance of mouse or human is readily evident.

Reporting for specific materials, systems and methods

We require information from authors about some types of materials, experimental systems and methods used in many studies. Here, indicate whether each material, system or method listed is relevant to your study. If you are not sure if a list item applies to your research, read the appropriate section before selecting a response.

Materials & experimental systems

n/a	Involved in the study
<input type="checkbox"/>	<input checked="" type="checkbox"/> Antibodies
<input checked="" type="checkbox"/>	<input type="checkbox"/> Eukaryotic cell lines
<input checked="" type="checkbox"/>	<input type="checkbox"/> Palaeontology
<input type="checkbox"/>	<input checked="" type="checkbox"/> Animals and other organisms
<input type="checkbox"/>	<input checked="" type="checkbox"/> Human research participants
<input checked="" type="checkbox"/>	<input type="checkbox"/> Clinical data

Methods

n/a	Involved in the study
<input checked="" type="checkbox"/>	<input type="checkbox"/> ChIP-seq
<input checked="" type="checkbox"/>	<input type="checkbox"/> Flow cytometry
<input checked="" type="checkbox"/>	<input type="checkbox"/> MRI-based neuroimaging

Antibodies

Antibodies used

REAGENT; SOURCE; CATALOG#; IDENTIFIER; LOT#; DILUTION
Mouse anti-TUJ1; BioLegend; Cat# 801201; AB_2313773; B264428; 1:500
Rat anti-SOX2; eBioscience; Cat# 14-9811-82; AB_11219471; 2023691; 1:50
Rabbit anti-SOX2; Cell Signaling Technology; Cat# 3579; AB_2195767; 01/2014 Lot:5; 1:50
Rabbit anti-KRT5; Abcam; Cat# ab52635; AB_869890; GR3198825-2; 1:1000
Rabbit anti-LHX2; Millipore Cat# ABE1402; AB_2722523; 3030529; 1:500
Rabbit anti-GNG13; Sigma; Cat# HPA046272; AB_10960062; R42082; 1:150
Rabbit anti-Ki67; Abcam; Cat# ab15580; AB_443209; GR3293897-3; 1:250
Rabbit anti-Doublecortin; Cell Signaling Technology; Cat# 4604; AB_561007; 08/2018; Lot:5 1:200
Mouse anti-OMP; Santa Cruz Biotechnology; Cat# sc-365818; AB_10842164; E1117; 1:500
Goat anti-OLIG2; R&D Systems; Cat# AF2418; AB_2157554; UPA0717121; 1:500
Mouse anti-TP63; Santa Cruz Biotechnology; Cat# sc-5301; AB_628093; D2519; 1:100
AlexaFluor 594 Goat anti-Mouse; Jackson ImmunoResearch; Cat# 115-585-146; AB_2338881; 109495; 1:100
AlexaFluor 488 Donkey anti-Mouse; Jackson ImmunoResearch; Cat# 715-545-150; AB_2340846; 113699; 1:100
AlexaFluor 594 Goat anti-Rabbit; Jackson ImmunoResearch; Cat# 111-585-144; AB_2307325; 106684; 1:100
AlexaFluor 488 Donkey anti-Rat; Jackson ImmunoResearch; Cat# 712-545-150; AB_2340683; 113383; 1:100
AlexaFluor 488 Donkey anti-Goat; Jackson ImmunoResearch; Cat# 705-545-147; AB_2336933; 115940; 1:100

Validation

The antibody TuJ-1 recognizes neuron-specific class III b tubulin. It does not react to the tubulin found in glia cells, and its reactivity in immature neurons has been well-described by our lab and others (Schwob et al., 1995; Goldstein and Schwob, 1996). Rat-anti SOX2 has been used widely in rodents in IHC and Western (Goldstein et al., 2016); we also validated identical nuclear cell type-specific labeling patterns in rodent or human compared to rabbit anti-SOX2. Rabbit anti-KRT5 has been shown

to react only to keratin 5 isoform in breast cancer cells; its cell type-specific labeling pattern in OE matches the patterns for antibody to KRT14 or another KRT5/6 antibody as published (Holbrook et al, 1995). Per manufacturer, rabbit anti-LHX2 antibody detected doxycycline-induced LHX2 expression in 10 µg of Murine keratinocyte K14rtTA-LHX2-TRE cell lysate. Rabbit anti-GNG13 has been shown in IHC in rodent to co-localize in olfactory neurons with markers labeling other known transduction proteins (AlMatrouk et al, 2018), and was validated by the Human Protein Atlas project. The rabbit anti-Ki67 has been reported extensively as a proliferative marker for human and rodent IHC. It produces identical labeling patterns with other Ki67 antibodies and has been shown to label proliferative cells from both mouse and human. The rabbit anti-Doublecortin recognizes a single appropriate band on Western blots from fetal rodent brain, and subventricular zone progenitor cells in developing mouse brain, and has been widely referenced. Mouse anti-OMP stains mature olfactory neurons with an identical pattern to a highly validated goat anti-OMP from WAKO that is no longer available. Goat anti-Olig2 recognizes a bHLH transcription factor in appropriate cell type-specific patterns in embryonic rodent tissue sections and was validated in ChIP reactions selectively detecting known Olig2 binding partners. It has also been verified to appropriately stain rat cortical progenitors in vitro with nuclear labeling pattern.

Animals and other organisms

Policy information about [studies involving animals; ARRIVE guidelines](#) recommended for reporting animal research

Laboratory animals	Tissue sections from male and female C57BL6 mice, 3 month old, were used for staining.
Wild animals	Study did not involve wild animals.
Field-collected samples	Study did not involve samples collected from the field.
Ethics oversight	Human tissue samples were obtained with patient informed consent and approval of the Human Subjects Research Office and the Institutional Review Board of the University of Miami. Animal work was approved by the Institutional Animal Care and Use Committee (IACUC), University of Miami.

Note that full information on the approval of the study protocol must also be provided in the manuscript.

Human research participants

Policy information about [studies involving human research participants](#)

Population characteristics	Total patients in study n = 7 Total patients with scRNA-seq data n = 4 Total patients with IHC data n = 6 Female n = 5 Male n = 2 Mean age: 42.29 (min 23 - max 52)
Recruitment	Patients were consented to provide tissue for research use from our population requiring endoscopic surgery involving approaches to the sphenoid sinus or anterior skull base, for problems not involving sinusitis, such that the nasal epithelium is uninvolves with any pathology. We excluded patients who have had prior surgeries, or vulnerable populations. There were no other specific exclusions or criteria that may introduce bias.
Ethics oversight	Human tissue samples were obtained with patient informed consent and approval of the Human Subjects Research Office and the Institutional Review Board of the University of Miami.

Note that full information on the approval of the study protocol must also be provided in the manuscript.